INTERNATIONAL JOURNAL FOR NUMERICAL METHODS IN FLUIDS, VOL. 12, 237–260 (1991)

VORTEX SIMULATION OF THE INTAKE FLOW IN A PLANAR PISTON–CHAMBER DEVICE

LUIS-FILIPE MARTINS AND AHMED F. GHONIEM
Massachusetts Institute of Technology, Cambridge, MA 02139, U.S.A.

SUMMARY

A numerical scheme based on the application of the vortex method to update the vorticity field and the implementation of the finite element method to satisfy the normal velocity boundary condition inside a complex time-dependent geometry is applied to simulate the flow produced by a piston sliding out of a chamber equipped with single or multiple intakes. This unsteady confined vortex flow is of interest in many applications. We use the idealization that the flow is incompressible, two-dimensional and planar and we analyse the results to study the flow during the intake process inside a model of an engine cylinder. The chamber top is fitted with an inlet channel, an inlet port or an inlet valve. In all cases when the intake channel axis coincides with that of the chamber, the flow in each side of the chamber consists essentially of two large counter-rotating eddies of almost the same size. The computed structures of these flows resemble qualitatively those which have been observed experimentally. The fluid motion is also computed for the case of a chamber equipped with an intake whose axis is not aligned with the chamber axis. In this case the flow at the end of the stroke is dominated by a single large eddy produced by the merging of the two eddies forming on the sides of the port.

KEY WORDS Vortex methods Recirculating flows Piston–cylinder

1. INTRODUCTION

The formation of large vortex structures in steady and unsteady internal flows has widely been observed at intermediate and high Reynolds numbers in experimental studies and numerical simulations.[1] The properties, characteristics and influence of these structures on the dynamics and mixing in open, continuous, steady flow have been well documented. However, in confined flows with time-dependent geometry there has been less effort in analysing the origin of these vortex structures, their properties and how they affect the flow. We are interested in developing a computational methodology for the analysis of confined vortex flows at different levels of idealization.

In this regard the work reported here has three goals: (1) to couple the vortex method used to compute the rotational velocity component and update the vorticity field with the finite element method required to solve the potential flow problem which arises in the implementation of the normal velocity boundary condition along the boundaries of the domain, in the solution of confined vortex flow problems; (2) to study, qualitatively and using simplified models of the enclosure geometry, the complex unsteady vortex flow which is encountered in piston–cylinder devices, e.g. internal combustion engines during the intake process and how the flow depends on various geometrical parameters; and (3) to explore, on the basis of the results of model computations, the potential and advantage of extending the methodology to different symmetries

0271–2091/91/030237–24$12.00

Received 12 October 1989
Revised 5 February 1990

and higher dimensions in order to capture more of the flow processes in physical applications. In the discussion to follow we expand on these goals.

The application of vortex methods to internal confined flow requires the satisfaction of conditions on the velocity both normal to the boundary of the domain and tangential to the solid part of the boundary. In incompressible flow one can show that satisfying the condition on the normal velocity component is equivalent to adding, everywhere in the field, a velocity component derived from a potential function which satisfies a Laplace equation with a Neumann boundary condition. In many applications of internal flow this represents a major component of the velocity field that should be accurately computed. Meanwhile, to make the numerical methodology most useful, one must allow a reasonable degree of freedom for the user to define the geometry of the flow boundaries without having to substantially change the computer program. In this paper we explore the use of the finite element method to obtain solutions for the potential flow problem associated with the application of the vortex method to internal confined flows. We also address questions which arise when the vortex method is applied in a time-dependent geometry.

The flow structure during the intake process of a device which consists of a piston that moves inside a chamber or a cylinder has been shown to be dominated by large-scale vortices that arise due to the separation of the incoming flow around zones of sudden expansion.[2–4] It has also been shown experimentally that the flow structure inside the chamber depends on the geometry of the intake, including the seat angle and the location of the intake axis with respect to the chamber centreline, the chamber width/piston stroke ratio, the shape of the cylinder head, the clearance volume between the piston and the top of the chamber at the beginning of the stroke, and the geometry of the piston face.

Experimental investigations of piston–cylinder flows, which may be used to systematically study the effects of all these variables, are not plentiful because of several reasons. Piston–cylinder flows are highly unsteady, three-dimensional, confined and occur within complex enclosures. To be able to make accurate temporally and spatially resolved measurements of the velocity field in idealized models of this flow is a major task that requires non-intrusive instruments with small probe volume and fast response.[5] A parametric study in which all the parameters that control piston–cylinder flow are varied may be economically prohibitive. Studies of some idealized flows in simplified geometries have been most helpful in determining some of the basic features of piston–cylinder flows.[6] Results of these experiments will be used here to qualitatively check the accuracy of the numerical solutions.

The development of a computational methodology for the integration of mathematical models that describe the flow processes in piston–chamber devices is thus an important companion to such experimental effort. Even when applied to idealized flow models in simplified configurations, the computational results can be used to gain some valuable insight into the fundamentals of confined vortex flows and the effect of various design parameters on the flow dynamics. The development and application of this methodology have been the subject of our effort over the past few years.[7] In this paper we describe part of this effort and report on the incompressible two-dimensional planar fluid motion during the intake process in an idealized geometry.

Results for a two-dimensional planar piston–chamber device are not expected to represent accurately the flow in a real device. However, we hope to show that (1) by applying numerical simulation methods to these flows one can gain some insight into their behaviour, even though it is only qualitative at this stage, and (2) results obtained from this model, which we consider as the first step towards the more comprehensive computations of a three-dimensional flow model, are encouraging. We use planar geometry for simplicity. It also allows the simulation of a flow generated using an off-centre intake which cannot be simulated in an axisymmetric geometry. Using this geometry in preliminary computational analysis is similar to performing experiments

on a square piston device: while it does not model all aspects of the flow in real devices, it can be used in research to gain some valuable experience and information about the real systems. Comparisons with experimental results will thus be limited to the qualitative large-scale features of the flow.

The paper is organized as follows. In Section 2 the governing equations used to model the flow during the intake process are introduced in both the momentum conservation form and in the vorticity transport form. The latter form is utilized in the construction of the vortex method, which is briefly described along with the application of the finite element method in Section 3. The application of the vortex method to a semi-confined domain requires a number of modifications, such as the use of different sheet lengths and core sizes. Results for the flow during the intake process in chambers fitted with several intake configurations are then described and discussed in Section 4. In Section 5 the new results of the paper are summarized and conclusions are presented.

2. THE GOVERNING EQUATIONS

The flow within the chamber is assumed to be incompressible. We also make the assumption that the flow is essentially two-dimensional and planar, limiting the solutions to the dynamics of the large-scale motion. The unsteady viscous flow equations are

$$\nabla \cdot \mathbf{u} = 0, \tag{1}$$

$$\frac{\partial u}{\partial t} + \mathbf{u} \cdot \nabla \mathbf{u} = -\nabla p + \frac{1}{Re} \nabla^2 \mathbf{u}, \tag{2}$$

where $\mathbf{u} = (u, v)$ is the velocity in the x- and y-directions respectively, normalized with respect to a reference velocity U_0; $\mathbf{x} = (x, y)$ is the spatial co-ordinate normalized with respect to a reference length D; y is the chamber axis and x is normal to the axis; t is time normalized with respect to D/U_0; p is pressure normalized with respect to ρU_0^2, where ρ is the density of the gas; $Re = U_0 D/\nu$ is the Reynolds number, where ν is the kinematic viscosity; and $\nabla = (\partial/\partial x, \partial/\partial y)$. The boundary conditions are: the velocity tangential to a solid wall is zero and the velocity normal to the boundary of the computational domain is prescribed as follows — it is zero on the chamber walls and equal to the piston velocity at the piston face and to the inlet flow velocity at the inlet section. The velocity at the inlet section is governed by the overall continuity condition

$$\frac{dV}{dt} + \int \mathbf{u} \cdot \mathbf{n} \, dA = 0, \tag{3}$$

where V is the total volume of the chamber and $\mathbf{n}$ is the unit vector normal to the local area element dA. This condition is used to relate the fluid velocity at the inlet section of the intake to the piston velocity. The velocity distribution across the inlet section of the intake, which constitutes part of the boundary of the computational domain, is taken to be uniform. The initial conditions are: at $t = 0$ the piston is stationary at its uppermost position close to the chamber top, and the velocity and vorticity everywhere are zero. The flow inside the chamber is driven by the motion of the piston away from the cylinder head.

The form of the governing equations which is used in the application of the vortex method is the vorticity transport form obtained by taking the curl of equation (2). If the vorticity is $\omega \mathbf{k} = \nabla \times \mathbf{u}$, where $\mathbf{k}$ is the unit vector normal to the x–y plane, then

$$\frac{d\omega}{dt} = \frac{1}{Re} \nabla^2 \omega, \tag{4}$$

where the Lagrangian derivative is $d/dt = \partial/\partial t + \mathbf{u} \cdot \nabla$. Using this formulation, the velocity can be computed directly from the vorticity field using the Biot–Savart law:

$$\mathbf{u}(\mathbf{x}) = \int \mathbf{k}(\mathbf{x} - \mathbf{x}')\, \omega(\mathbf{x}')\, d\mathbf{x}' + \nabla\phi, \tag{5}$$

where $\mathbf{k}(\mathbf{x}) = (1/2\pi)(-y, x)/r^2$ is the kernel of the Poisson equation, $r = |\mathbf{x}|$ and $\nabla\phi$ is a potential velocity which satisfies the conditions imposed on the velocity component normal to the boundary of the computational domain. The first term on the right-hand side of equation (5) is the vortical velocity $\mathbf{u}_\omega$, which satisfies the following two conditions: $\nabla \cdot \mathbf{u}_\omega = 0$ and $\nabla \times \mathbf{u}_\omega = \omega\mathbf{k}$. For the potential velocity component one can easily show that ϕ satisfies the following conditions:

$$\nabla^2\phi = 0 \tag{6}$$

and

$$\frac{\partial\phi}{\partial n}(s, t) = (\mathbf{U}_b - \mathbf{u}_{\omega, \partial D}) \cdot \mathbf{n}, \tag{7}$$

where s is a parameter which defines the boundary ∂D of the domain, $\mathbf{U}_b$ is the prescribed velocity of the boundary and $\mathbf{u}_{\omega, \partial D}$ is the vortical component of the velocity computed at the boundary.

The no-slip condition on the solid walls is satisfied by generating vorticity at the magnitude of $\Gamma(s, t) = -\int \mathbf{u}_{\partial D} \cdot \mathbf{s}\, ds$, where $\mathbf{s}$ is the unit vector tangential to the solid wall and parallel to ds, and $\mathbf{u}_{\partial D}$ is the velocity produced by the existing vorticity field, the inlet flow and the motion of the boundaries of the domain. This vorticity is added to the field along the solid walls in the form of a vortex sheet and is allowed to participate in the motion in the subsequent time steps.

3. THE NUMERICAL SCHEME

In the vortex method the vorticity field is discretized into a number N of vortex elements. Each element carries a uniform vorticity distribution ω_i of radially symmetric extent δ away from the centre of the element. The total circulation of each element, $\Gamma_i = \pi\delta^2\omega_i$, remains constant along the element trajectory $\chi_i(t)$, which is determined by the solution of the vorticity transport equation. Thus the vorticity at any moment is given by

$$\omega(\mathbf{x}, t) = \sum_{i=1}^{N} \Gamma_i f_\delta(\mathbf{x} - \chi_i(t)), \tag{8}$$

where $f_\delta = 1/\pi\delta^2$ for $r/\delta \leqslant 1$ and $f_\delta = 0$ for $r/\delta > 1$. The element trajectory $\chi_i(t)$ is derived from an approximate solution of the vorticity transport equation, equation (4), on the basis of viscous splitting.[8,9] This fractional step scheme allows one to decompose the total displacement of an element of vorticity into a convective transport along a particle path and a diffusive transport which is proportional to the square root of the molecular diffusivity. Utilizing the random walk algorithm for the solution of the diffusion equation,[10,11] the vortex element trajectory can be written as

$$\chi_i(t + \Delta t) = \chi_i(t) + \int \mathbf{u}(\chi_i, t)\, dt + \eta_i, \tag{9}$$

where η_i is a two-component Gaussian random variable of zero mean and standard deviation equal to $(\sqrt{2\Delta t/R})$, used to stochastically simulate the diffusion displacement. The velocity is

computed by substituting the discrete vorticity distribution, equation (8), into equation (5). The resulting expression is a summation over the velocity field induced by individual vortex elements:

$$\mathbf{u}(\mathbf{x}) = \sum_{i=1}^{N} \Gamma_i \mathbf{K}(\mathbf{x} - \boldsymbol{\chi}_i)\, \kappa_\delta(\boldsymbol{\chi}_i) + \nabla\phi, \tag{10}$$

where $\kappa_\delta = 2\pi \int f_\delta r\, dr$. For the Rankine vortex core used in this work, $\kappa_\delta = 1$ for $r/\delta > 1$ and $\kappa_\delta = r^2/\delta^2$ for $r/\delta < 1$.

The potential velocity component $\nabla\phi$ is computed using a finite element solution of the Laplace equation governing ϕ with a Neumann boundary condition. The choice of this method to solve the potential flow problem was based on its relative simplicity and flexibility in handling complicated boundary configurations such as those encountered in piston–cylinder devices. The solution is constructed to satisfy the condition that the velocity normal to the boundaries of the computational domain is zero if the wall is stationary and fnite if the wall is moving or if the flow is penetrating a part of the boundary such as the inlet section. The appropriate formulation of the finite element solution thus utilizes a Neumann boundary condition.

We note that equations (6) and (7) determine the solution of ϕ only to within an additive constant. This, however, does not violate the uniqueness of the velocity which is defined by $\nabla\phi$. Moreover, for a solution ϕ to exist, the following compatibility condition must be satisfied:

$$\int_{\partial D} \frac{\partial \phi}{\partial n}\, ds = 0. \tag{11}$$

This relationship is simply the principle of conservation of mass (volume in the incompressible flow case) for the entire domain. It is easy to show that $\int_{\partial D} \mathbf{u}_\omega \cdot \mathbf{n}\, ds = 0$.

To reduce the continuum boundary value problem which arises in the implementation of the normal velocity boundary condition to a finite set of algebraic equations, we employed the Galerkin weighted residual process together with a finite element discretization of the domain.[12] In this work we use linear triangular elements with mesh refinement around sharp corners. Since the Neumann problem in ϕ is defined up to a constant, the stiffness matrix of the finite element formulation is singular. To overcome this difficulty, the value of ϕ is prescribed at one mesh nodal point before the matrix is inverted. Finally, the potential velocity component is obtained by differentiating the discrete solution within each element. The resolution of the potential flow problem is governed by the size of the finite elements since the potential velocity is constant across an element.

The no-slip boundary condition is satisfied by computing the slip velocity $u_{s,\partial D}$ along the walls at points separated by a distance h along each wall at each time step of the computations.[10,13] In an unsteady motion a slip velocity arises owing to the combined effect of (1) the existing vorticity field, (2) the flow across the boundaries of the domain and (3) the flow associated with the motion of the boundaries of the domain. A new vortex element is created when the circulation generated by the slip, $\Gamma_j = -u_s h$, exceeds a small threshold value selected on the basis of the desired resolution. If Γ_j exceeds a maximum value, several elements are created at this point on the boundary. In the next time step the new elements are allowed to participate in the motion by first diffusing into the interior field and then getting convected by the existing velocity field.

A complex methodology known as the vortex sheet algorithm[13] has been developed on the basis of utilizing vortex sheets which are aligned parallel to the wall in the zone very close to the boundary to improve the resolution.[13,14] The vortex sheet algorithm utilizes the conveniences of the boundary layer approximation within a distance $\Delta_s = O(\sqrt{\Delta t/R})$ normal to the walls. Vortex sheets have length equal to h and circulation per unit length equal to $-u_s$. Vortex blobs are generated when a vortex sheet moves out of the zone Δ_s. The circulation of a vortex blob equals

that of the vortex sheet, while its core radius is taken as $h/2$ to satisfy the overlap condition. This methodology has been described in detail in Reference 15.

Before presenting results on the application of the vortex method to the confined vortex flow inside a model of a piston–chamber device, we should mention that extensive theoretical and numerical studies have been conducted to investigate the convergence and accuracy of the vortex method. Most noteworthy is the theoretical work of Hald[16] and Beale and Majda[17] on the convergence of the inviscid methods, the work of Marchioro and Pulvirenti[18] and Long[19] on the convergence of the random vortex method, and the work of Hald[20] on the convergence of the vorticity creation algorithm in some special cases. Numerical experiments by Roberts[21] used simple flows whose evolution can be written analytically to check the results of the theoretical analysis. Numerical experiments by Puckett[22] investigated the convergence of the vortex sheet algorithm for the solution of the boundary layer equations.

Detailed numerical simulations of steady separating flow in Reference 15 and unsteady separating flow in Reference 23 were also used to investigate the properties of the vortex algorithm. Experimental data were used to check on the accuracy of the numerical solution of shear flows and recirculating flows.[24,25] Numerical convergence studies were performed to find the optimum set of numerical parameters to be used to achieve high accuracy without sacrificing efficiency. Conclusions of these studies were implemented in the current work. Other separating flow studies using the vortex method were performed by Ashurst,[26] Peskin and McCracken[27] and Cheer.[28]

Application of vortex methods to internal confined flows were presented before by Chorin[13] and Ashurst[29] for a geometry similar to the configuration used in our work and by Sethian[30] for a closed cavity. Chorin[13] combined the vortex sheet algorithm with the random choice method to simulate this flow. In Ashurst's work[29] the no-slip condition on the walls was not satisfied and the inlet flow was aproximately represented by introducing vortices at a point where the separation at the valve would have occurred, i.e. the actual valve was not represented. It was also assumed that the Reynolds number is infinity and the inlet boundary layer is infinitely thin. In our computations the Reynolds number is finite, the no-slip condition along all solid walls is satisfied and the geometry of the valve is represented without any additional approximations. It should be emphasized that recent numerical simulations of piston–cylinder flows showed a very clear difference between inviscid and viscous flow computations. Hybrid methods in which the vortex method was used near the boundaries and the finite difference method or the random choice method was used in the interior were also devised for confined flow by Chorin[13] and Sod.[31,32] Choi *et al.*[33] utilized the vortex sheet–random vortex method to investigate the unsteady dynamics in a confined cavity flow.

Several issues unique to computing a confined flow using the vortex method are worth addressing before we present the results.

(1) In satisfying the no-slip conditions on the walls, one must select a number of points along each wall to compute the circulation of the new elements. If the length of the wall changes with time, the length of vortex sheets also changes by the same ratio, i.e. we keep the number of check points on the wall constant while changing the distance between the points, h, each time step. The length of a vortex sheet does not change once it is generated, and hence at any moment, vortex sheets with different lengths may coexist to satisfy the no-slip boundary condition.

(2) The core radius of a vortex blob, which depends on the length of the vortex sheet which was transformed into that blob, is determined according to the length of the vortex sheet. Since the flow is incompressible, the size of the core of a vortex blob remains constant. Thus vortex blobs of different core radii may coexist within the interior of the domain.

(3) The finite element mesh used to solve the potential flow problem changes every time step to accommodate the computational domain which expands in the y-direction. This is done only within the chamber cavity since the intake has fixed dimensions. The aspect ratio of the element changes since only one side is expanding and care must be exercised in order not to lose accuracy by using elements with large aspect ratio. The only terms that change in the stiffness matrix are those associated with differences in the y-co-ordinates of the nodes.

(4) A limit on the time step should be enforced to achieve high accuracy in satisfying the no-slip boundary condition. This time step limit can be determined using the following criterion:

$$\Delta t \leqslant 0{\cdot}5 \frac{h_{\min}}{N_s U_m}, \tag{12}$$

where U_m is the maximum velocity within the domain, N_s is the number of sheets generated at the point where the slip velocity is U_m and $h_{\min}$ is the shortest sheet length. As we mentioned before, a number of vortex sheets, N_s, may be generated at a point if the slip velocity is too high to improve the resolution in the normal-to-the-wall direction. Using this criterion, the displacement of the vortex sheet in the first time step after it has been created, which upsets the no-slip condition by a factor proportional to U_m/N_s, will not exceed one-half of its length. Note that both h and the maximum velocity change with time and that $h \sim (L_c + \int_0^t u_p \, dt)/N_w$, where L_c is the distance between the chamber head and the piston face at the beginning of the stroke, i.e. the clearance height, u_p is the piston velocity and N_w is the number of check points on side wall of the chamber where the slip velocity is computed and vortex sheets are generated. If $U_m \sim u_p$ is approximately constant, then

$$\Delta t \leqslant \frac{1}{2N_w N_s} \left(\frac{L_c}{u_p} + t \right). \tag{13}$$

Thus the smallest time step is the first step, $\Delta t = L_c/2N_w N_s u_p(\Delta t)$. In actual computations we used a fixed time step during the stroke as shown in the discussion of the results.

4. RESULTS

In this section we discuss results of the application of the vortex–finite element method to study the flow during the intake process inside a chamber. The flow is produced by moving a piston away from the chamber head according to a simple harmonic motion, i.e. the piston is motored in a way similar to that used in experimental studies.[4, 6] The motion of the piston follows a cosine wave while its velocity follows a sine wave. In the presentation of results, the chamber width D and the maximum piston velocity U_0 were used to normalize the length and velocity respectively. In all cases the clearance height is $L_c/D = 0{\cdot}15$, except for the case with a valve in which $L_c/D = 0{\cdot}25$, and the piston stroke is $L_s/D = 1{\cdot}5$.

For most runs the Reynolds number $Re = U_0 D/\nu$ was taken as $Re = 350$. In all cases we insisted that the velocity distribution at the exit of the incoming channel and at the chamber head be fully developed. To achieve this, the length of the inlet channel between the boundary of the computational domain and the inlet to the chamber had to be adjusted as the Reynolds number was increased. With a short inlet channel $L_i/D = 0{\cdot}225$, where L_i is the length of the inlet channel, the velocity profile at the chamber inlet became almost fully developed at this Reynolds number. When we increased the Reynolds number to $Re = 3500$, we had to increase the length of the inlet channel to $L_i/D = 1{\cdot}26$ to recover a fully developed velocity profile at the inlet of the chamber. When the inlet velocity profile across the chamber inlet was fully developed, the effect of the Reynolds number on the flow structure inside the chamber was relatively small. At higher

Reynolds number the vortex structures became more coherent and less diffusive. In this paper we will concentrate on the results of the $Re = 350$ case. The weak effect of the Reynolds number was observed in experimental results.[4, 2]

In all cases we used the following set of numerical parameters. The number of segments where sheets are generated to satisfy the no-slip condition is as follows: along the incoming channel walls, 4; along each of the side walls, 12; along the piston head, 5; and along each part of the chamber head on the two sides of the inlet, 2. The length of the sheets on different walls was adjusted to fit an integer number of sheets on the wall. The maximum vorticity per sheet is $h_i/3{\cdot}0$, where h_i is the sheet length. The sheet layer thickness is 1·5 times the random walk standard deviation. The time step is determined by dividing the time of a stroke into 200 steps. It is equal to 0·0106 for all cases except for the case of a piston with a valve for which $\Delta t = 0{\cdot}00982$. The integration scheme for the motion of the vortex blobs is second-order. The average number of blobs within the domain at the last time step was 4500.

Numerical results were obtained for four cases: (1) a chamber fitted with *an inlet channel* centred around its axis; (2) a chamber fitted with *an inlet port* which consists of two channels inclined with respect to the chamber head at 30° and 60°; (3) a chamber fitted with *an inlet valve* centred around its axis with a seat angle of 45°; and (4) a chamber fitted with *an inlet port* centred between the left wall and the centreline of the chamber with an equivalent seat angle of 30°. The first three cases were chosen to match conditions used in different experimental investigations published in the literature. To match the conditions of the experimental investigations, symmetry was imposed across the chamber centreline. Qualitative comparisons with experimental data are made to validate these results. The last case was simulated to find out whether a coherent vortical motion with a single sense of rotation may be induced by an off-centre intake port. In all cases the valve or the port was assumed to be fully open during the entire stroke.

For each case we show the results in terms of the instantaneous location and velocity of all the vortex elements used in the computation, the instantaneous velocity distribution computed on a uniform grid within the chamber, and the instantaneous streamlines. These data are shown for four values of the angle of the sine wave as the piston moves away from the chamber head. The angles $\theta = 45°, 90°, 135°$ and 180° correspond to quarter stroke, half stroke, three-quarters stroke and full stroke respectively.

The plots of the location of the vortex elements are utilized to indicate the relative intensity of vorticity within the chamber since all vortex elements are assigned the same absolute value of vorticity. The instantaneous velocity vectors of the vortex elements show how the vorticity field is clustered into distinct structures that exhibit different degrees of coherence as the piston moves away from the chamber head. They also show the sense of rotation of the large structures.

The instantaneous velocity on a uniform grid is shown to demonstrate the velocity distribution across any given cross-section within the chamber. The streamlines are shown to identify the boundaries of the vortex structures and to determine the volumetric entrainment of fluid inside the structures. The difference between the values of the streamfunction on the outer boundary and at the centre of the structure is a measure of how much fluid is trapped within this structure. The streamline plots are also used to compare the numerical results with the experimental data which are most often presented in this form.

Two major differences between the numerical results and the experimental measurements are the overall symmetry of the flow and the type of averaging performed on the results. In the numerical simulations we assumed that the flow was planar and imposed symmetry across the centreline of the chamber, while in the experiment the flow was, on the average, radially symmetric. Moreover, while instantaneous unaveraged quantities, within the given temporal and spatial resolution of the numerical scheme, are shown for the numerical solution, flow variables

which are averaged over an ensemble of many realizations or many cycles are used to document the experimental results, except when flow visualization was used to identify the structures.

4.1. A chamber fitted with an inlet channel

Figures 1–3 show the numerical results for the case in which the intake is a channel whose centreline is aligned with that of the chamber. The ratio between the width of the channel and that of the chamber is $d/D = 0{\cdot}2$. Results in Figure 1, depicting the vortex elements and their velocities, show that at early stages the inlet jet rolls up into two large eddies on both sides of the centreline. Since the flow is symmetric, we will discuss results of one side only. The first eddy to form, which we call the valve eddy, entrains most of the jet fluid and some of the fluid which existed in the chamber before the piston started to move. The valve eddy forms owing to the separation of the inlet jet at the point of sudden expansion between the inlet channel and the main chamber. Since the jet fluid moves faster than the piston face, the valve eddy soon collides with the face of the moving piston. The impact of the inlet jet on the moving piston is due to the difference between their velocities, as defined by the area ratio d/D, which persists throughout the entire stroke. The presence of the valve eddy at these early stages indicates that its formation and direction of rotation are induced by the separation of the inlet jet and not by the piston. However, the growth of the valve eddy is confined by the piston. The presence of the eddy is clear at crank angle $\theta = 45°$.

As soon as it collides with the piston, the jet bifurcates into two streams which move along the piston face towards the respective side walls. The streams are then deflected when they collide with the side walls and start to move along the walls towards the chamber head. The motion of the jet on both sides of the centreline is consistent with the sense of rotation of the valve eddies. Results at $\theta = 90°$ indicate that the action of the jet, in terms of its motion along the piston face and the side walls, contributes to the growth of the eddy which now fills the entire chamber. The centre of the eddy, being almost halfway between the chamber head and the piston face but closer to the latter, follows the motion of the piston. Meanwhile, a counter-rotating corner eddy is developing between the chamber head and each of the two side walls. Notice the thick, highly

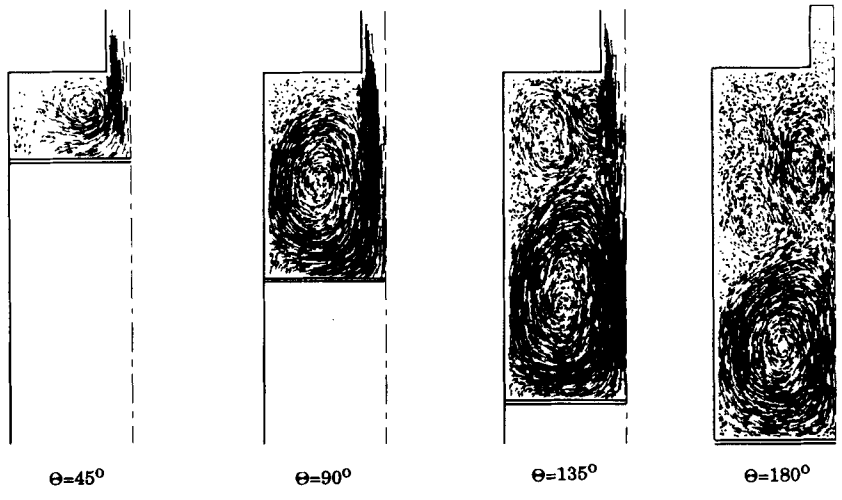

Figure 1. The symmetric flow field, depicted in terms of the vortex elements, shown as solid circles, and their instantaneous velocity vectors, shown as lines starting at the vortex element centres, for the intake flow in a planar piston–chamber device fitted with a centred inlet channel, shown at equivalent crank angles $\theta = 45°$, 90°, 135° and 180°

concentrated zone of vorticity which constitutes the core of the jet and covers the length of the chamber all the way from the inlet to the piston face. Clearly, most of the vorticity within the chamber is produced in the inlet channel and is carried by the jet into the chamber.

For $\theta > 90°$ the piston starts to slow down and the valve eddy starts to move away from the chamber head, following the piston motion. The inlet jet rolls up to form a new valve eddy which rotates in the same direction as the original valve eddy. For $90° > \theta > 135°$ part of the inlet jet still contributes to the growth of the original valve eddy and the other part is entrained by the new valve eddy. Meanwhile, the corner eddy grows to fill the area between the valve eddy and the chamber walls. The vorticity within the corner eddy is counter-clockwise. Contrary to the valve eddies, the vorticity in the corner eddy is generated on the walls of the chamber. As shown by the results in Figures 1–3, a stagnation point exists between the two valve eddies and the corner eddy. For $135° > \theta > 180°$ more counter-clockwise vorticity is generated along the walls of the chamber, contributing to the decay of the original valve eddy. The slow decay of the valve eddy continues until the end of the intake stroke.

The relative magnitudes of the velocity on an expanding mesh and at different stages are shown in Figure 2. By $\theta = 45°$ the valve eddy has already been formed with its centre closer to the chamber head than to the piston face. This confirms that the formation of the valve eddy is due to the separation of the inlet jet at the point of sudden expansion and not due to the impact of the jet on the piston face. As soon as the valve eddy expands to reach the side walls, the corner eddy starts to form owing to the generation of vorticity opposite to that of the valve eddy on the side walls of the chamber. The growth of the original valve eddy slows down substantially beyond $\theta > 90°$ while a new valve eddy forms at the separation point. Moreover, the corner eddy grows as

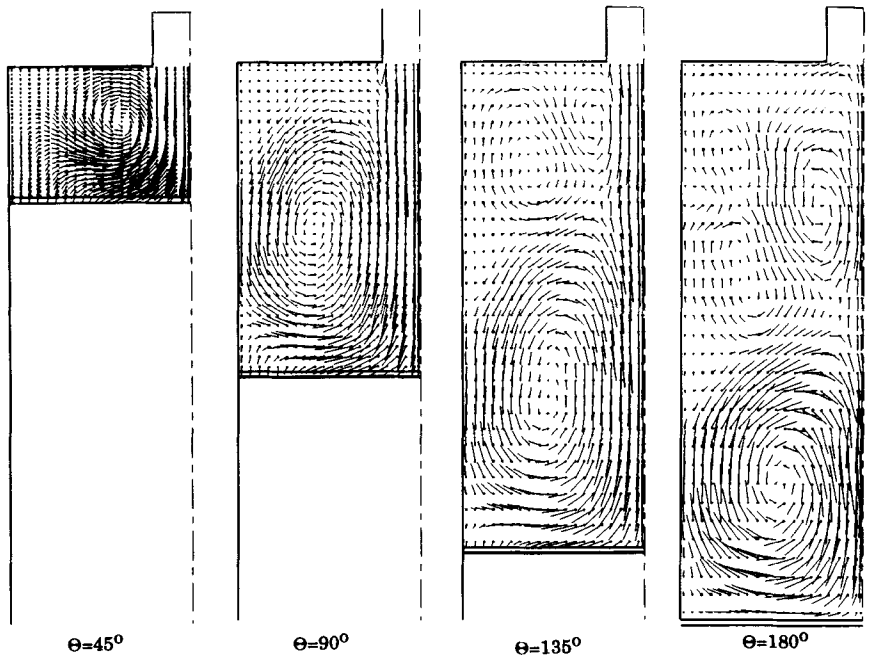

Figure 2. The symmetric flow field, exhibited in terms of the instantaneous velocity vectors on a uniform expanding grid, for the intake flow in a planar piston–chamber device fitted with a centred inlet channel, presented at equivalent crank angles $\theta = 45°$, 90°, 135° and 180°

the boundary layer on the side wall rolls at the corner. The figure shows that the velocities within the corner eddy are much smaller than within the valve eddy, while the velocities within the jet region are much higher than those within the valve eddy. The figure also shows the presence of the stagnation point between the large eddies for $\theta > 90°$.

Figure 3 shows the streamlines constructed from the velocity distribution in Figure 2. These plots compare favourably with the streamlines constructed from experimental meausrements of velocity in the work of Durst *et al.*[4] and Morse *et al.*,[5] although the symmetry of the numerical solution is different from that of the experiments. The figure shows that the start of the corner eddy occurs soon after the piston is set into motion. However, it becomes detached from the chamber head to develop into a separate structure after $\theta = 90°$. The streamlines also show that even after the formation of the corner eddy, the valve eddy remains as the major structure in the field. The concentration of the sreamlines indicates that the valve eddy maintains most of its energy as it is pulled by the piston motion. Meanwhile, its size increases as more of the jet fluid swirls around its centre.

4.2. A chamber fitted with a centred port

Figures 4–6 show results for the case when the chamber head is fitted with an inlet port which consists of two channels inclined with respect to the chamber head at 30°. The two channels are positioned symmetrically around the centreline of the chamber. The centreline of each inlet

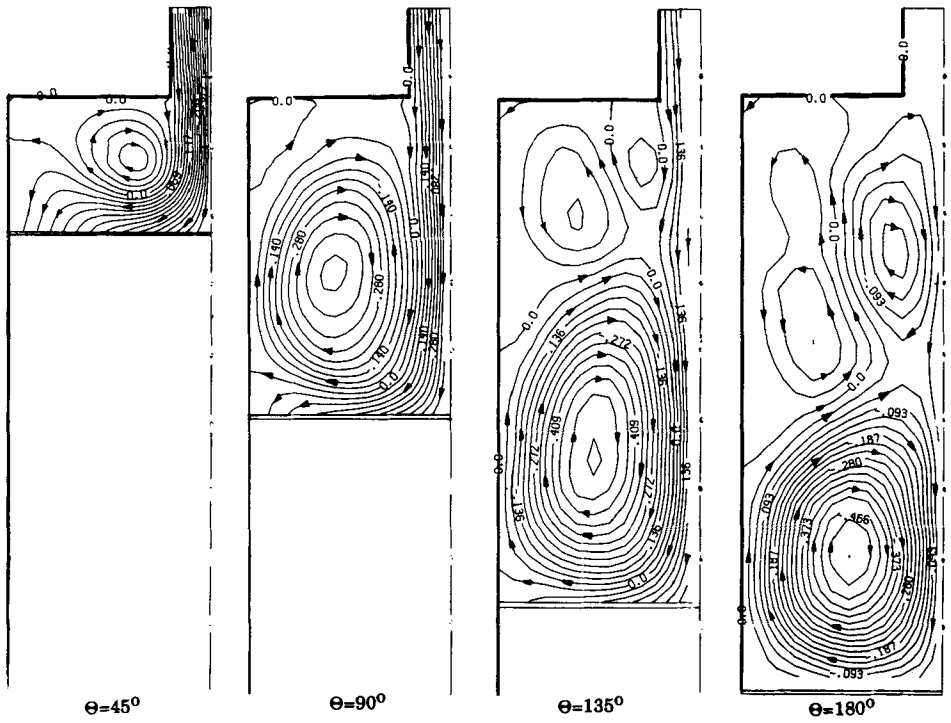

Figure 3. The symmetric flow field, illustrated by the instantaneous streamlines, for the intake flow in a planar piston–chamber device fitted with a centred inlet channel, shown at equivalent crank angles $\theta = 45°$, 90°, 135° and 180°.

channel is located halfway between the chamber wall and the chamber centreline. The width of each channel is $d/D=0{\cdot}125$, where d is measured along the chamber top.

The position and velocity of the vortex elements, shown in Figure 4, indicate that at the early stages and until $\theta=45°$ the jet flow in the chamber is directed normal to the piston face and that the jet centreline is positioned halfway between the chamber wall and its centreline. This motion is created by the separation of the inlet jet on both sides of the inlet channel and the formation of a strong separation eddy between the chamber centreline and the inlet channel (owing to the imposed symmetry, another eddy forms on the other side of the chamber centerline). This valve eddy entrains all the inlet jet fluid and its centre is almost halfway between the chamber head and the piston face. Meanwhile, two smaller eddies, which rotate in the opposite direction to the valve eddy, form between the piston face and the chamber side wall; the piston eddy and, between the valve eddy and the corner at the chamber head, the corner eddy.

Beyond $\theta=45°$ the inlet jet becomes essentially aligned with the inlet channel. The growth of the valve eddy by entraining the incoming jet fluid forces the jet to move towards the side wall of the chamber and to become aligned with the direction of the inlet channel. The jet stream, after getting deflected from the side wall, moves along this wall, the piston face and around the valve eddy. For $45°<\theta<90°$ the valve eddy fills the entire chamber cavity and its centre moves in tandem with the piston. The deflection of the jet towards the side wall by the presence of the valve eddy confines the corner eddy to a very small space near the chamber head. On each side of the symmetry line the motion of the jet along the chamber wall supports the growth of a boundary layer between the chamber head and the piston face. As the piston decelerates, $\theta>90°$, this boundary layer separates from the chamber wall. The separating boundary layer rolls up and joins the piston eddy. We note that the vorticity generated within the boundary layer along the chamber wall is opposite to the vorticity which forms the valve eddy.

With the deceleration of the piston beyond half crank, $90°<\theta<135°$, the valve eddy grows very slowly. Meanwhile, the piston eddy grows to fill the space between the valve eddy and the piston face. The jet fluid itself moves along the outer edges of the valve eddy, along the chamber wall and seems to split into two parts; one part is entrained by the valve eddy and the other is entrained by

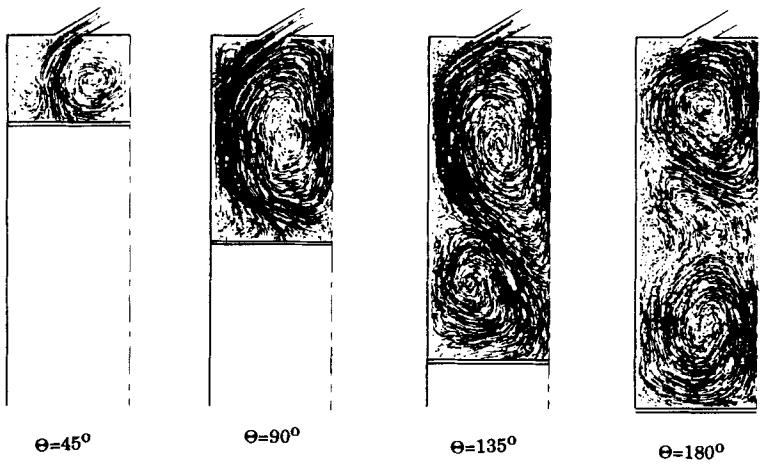

Figure 4. The symmetric flow field, depicted in terms of the vortex elements and their instantaneous velocity vectors, for the intake flow in a planar piston–chamber device fitted with a centred intake port at an equivalent seat angle of 30° with the chamber head, shown at equivalent crank angles $\theta=45°$, 90°, 135° and 180°

the piston eddy. This dynamics suggests that the fresh charge is divided into two parts during the intake process. The early part of the fresh charge stays on the top part of the chamber and near the chamber head while the latter part accumulates in the bottom part and near the piston. The mixing between these two almost stratified parts of the charge is not accomplished during the intake stroke and is somewhat inhibited by the presence of the two large eddies.

With further deceleration of the piston, $135° < \theta < 180°$, the coherence of the value eddy gradually deteriorates while the piston eddy grows by entraining some of the fluid leaking from the valve eddy and from the penetrating jet. The valve eddy becomes smaller and moves closer to the chamber head. Meanwhile, the piston eddy remains almost stationary while its size is expanding. The plots of the vortex elements and their velocity indicate that by the end of the intake stroke only two-thirds of the volume of the chamber charge is actually part of a coherent motion. The dissipation of kinetic energy due to the shear between the neighbouring counter-rotating large eddies, or equivalently the diffusion of vorticity of different signs, and between the eddies, the chamber wall and the jet stream overcomes the initial coherent motion within the dominant two large eddies and turns it into a weakly organized motion.

The development of the large vortical structures is seen clearly from the plots of the magnitude and direction of the velocity vectors on a uniform expanding grid in Figure 5. In these plots the different stages of the three distinct eddies, the corner eddy, the valve eddy and the piston eddy, can be followed. It is also noted that, while by the end of the intake stroke the orders of magnitude of the velocities within the chamber are not changed from their values at mid-stroke, the two main eddies are smaller and the flow is losing its organization.

The plots of the streamlines show that the highest velocities are attained between $\theta = 45°$ and 135° when the incoming jet is directed by the valve eddy. They also indicate that the jet path

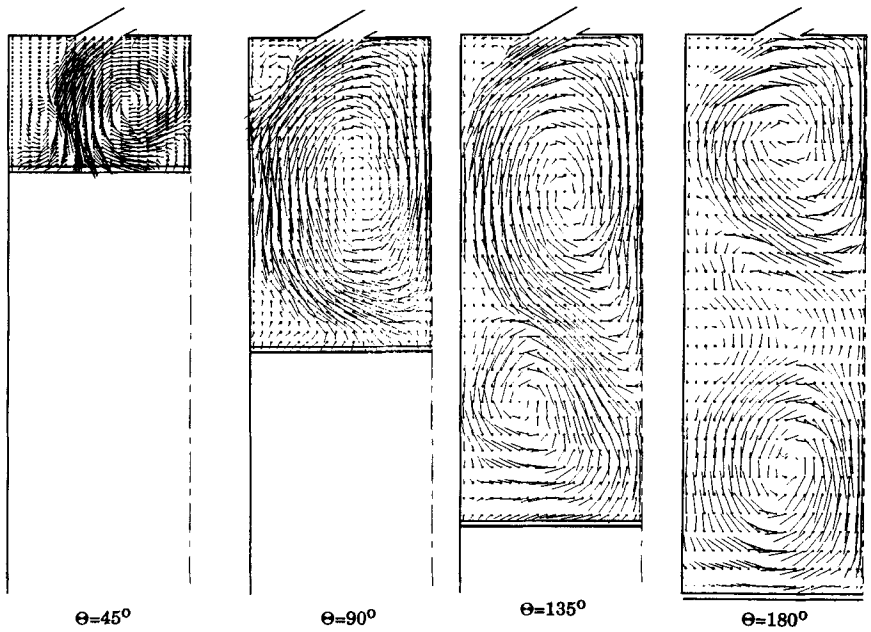

Figure 5. The symmetric flow field, exhibited in terms of the instantaneous velocity vectors on a uniform expanding grid, for the intake flow in a planar piston–chamber device fitted with a centred intake port at an equivalent seat angle of 30° with the chamber head, presented at equivalent crank angles $\theta = 45°$, 90°, 135° and 180°

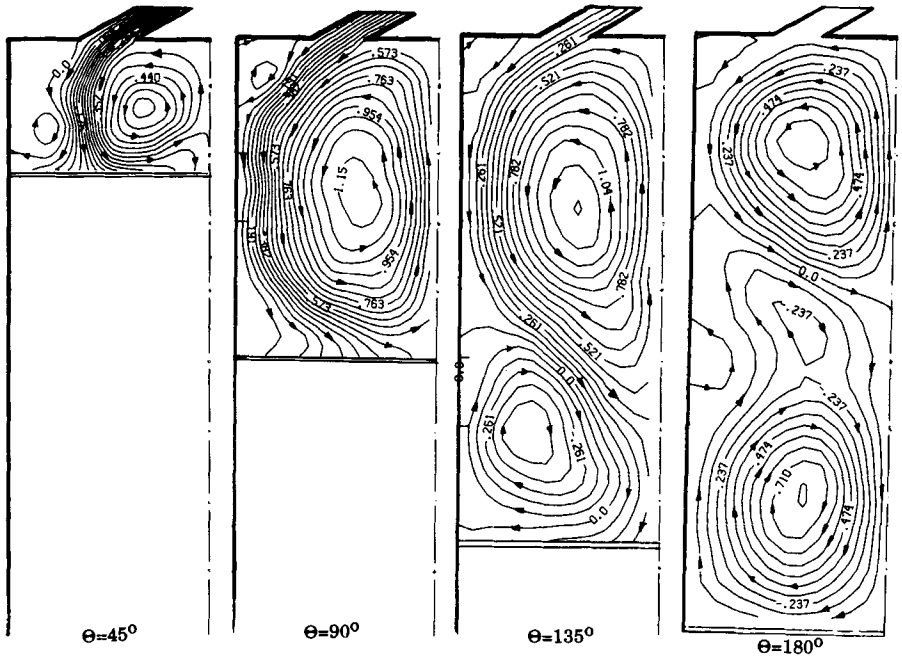

Figure 6. The symmetric flow field, illustrated by the instantaneous streamlines, for the intake flow in a planar piston–chamber device fitted with a centred intake port at an equivalent seat angle of 30° with the chamber head, shown at equivalent crank angles $\theta = 45°$, 90°, 135° and 180°

during this period is aligned with the inlet channel and is acting as a wall scavenger. At the late stages the values of the velocity decline and only a small fraction of the fluid within the chamber is trapped in the two counter-rotating large eddies. As observed before, the friction between the eddies and the chamber wall and between the neighbouring eddies continues to dissipate the flow energy and weaken the coherence which was seen in the early stages of the intake stroke.

An experimental study conducted by Morse *et al.*[5] and performed on a similar but axisymmetric configuration revealed a similar temporal and spatial development of the flow structure. Gosman[34] and El-Tahry[35] obtained similar results for the axisymmetric flow using finite difference methods with turbulence closure models. In the numerical and the experimental studies the three large eddies which we have seen in our numerical simulations were identified: the corner eddy, the valve eddy and the piston eddy. Our numerical simulations and the experimental data show, qualitatively, similar time evolution of the sizes and locations of the eddies. Further comparisons between our numerical simulations and the experimental measurements will be conducted when the former are extended to axisymmetric geometry, a task which we have undertaken.

To study the effect of the intake port angle on the flow field, simulations were performed for intake channels with an angle of 60°. In this case $d/D = 0{\cdot}075$. Results are plotted in Figures 7–9. As in the previous case, during the early stages the inlet jet moves normal to the piston head. Within the range $\theta = 45°$–$135°$ the inlet jet is aligned with the intake channel, i.e. at 60° angle with respect to the chamber head, separating the valve eddy from the corner eddy. After colliding with the chamber walls the jet moves along the side walls, creating a zone of very strong shear, a wall boundary layer. Because of the larger seat angle, the corner eddy is larger than before but is still

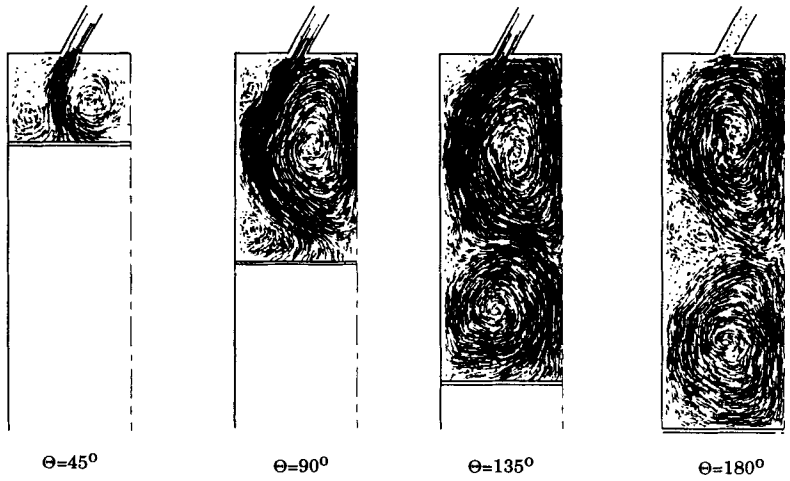

Figure 7. The symmetric flow field, depicted in terms of the vortex elements and their instantaneous velocity vectors, for the intake flow in a planar piston–chamber device fitted with a centred intake port at an equivalent seat angle of 60° with the chamber head, shown at equivalent crank angles $\theta = 45°$, 90°, 135° and 180°

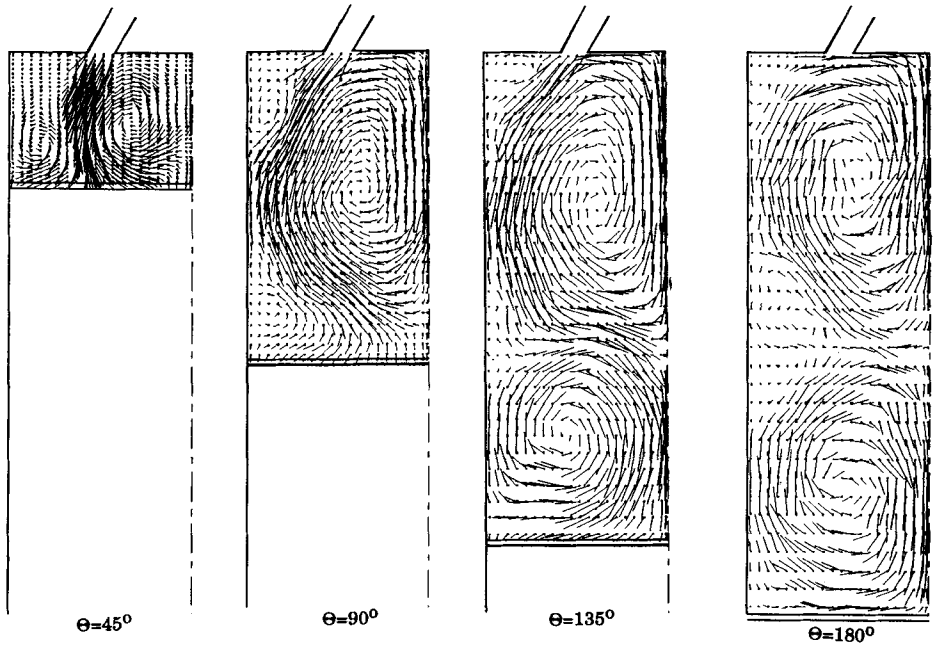

Figure 8. The symmetric flow field, exhibited in terms of the instantaneous velocity vectors on an expanding uniform grid, for the intake flow in a planar piston–chamber device fitted with a centred intake port at an equivalent seat angle of 60° with the chamber head, presented at equivalent crank angles $\theta = 45°$, 90°, 135° and 180°

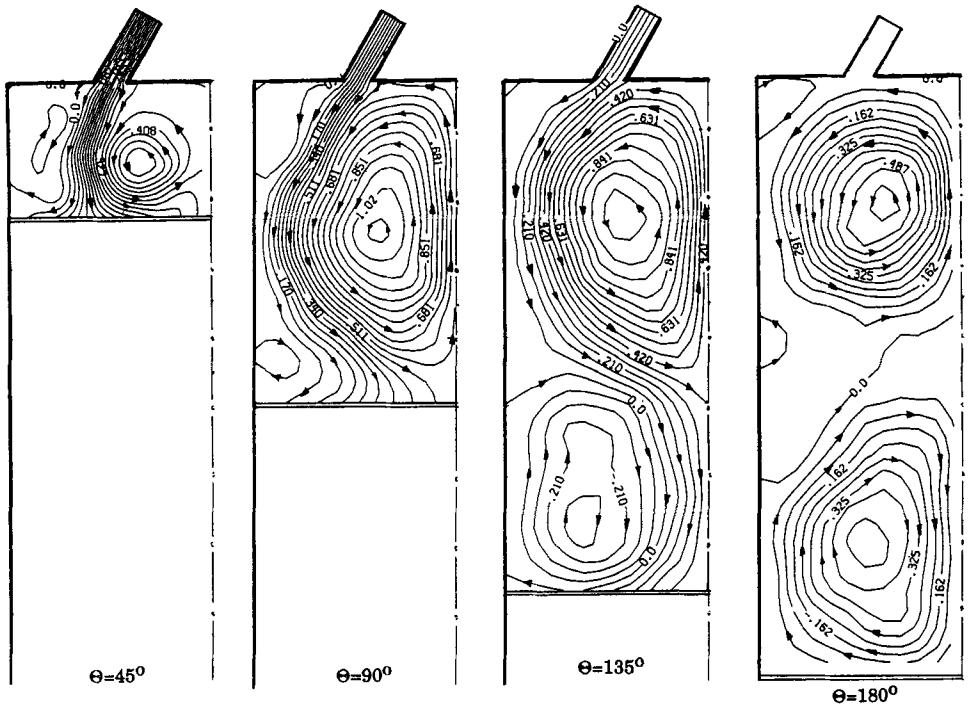

Figure 9. The symmetric flow field, illustrated by the instantaneous streamlines, for the intake flow in a planar piston–chamber device fitted with a centred intake port at an equivalent seat angle of 60° with the chamber head, shown at equivalent crank angles $\theta = 45°$, 90°, 135° and 180°

weak and relatively uninfluential. Beyond $\theta > 90°$ the vorticity within the side wall boundary layer is swept by the penetrating jet into the piston eddy. As the piston reaches a crank angle $\theta = 135°$ the chamber is filled with a fresh charge which is trapped into one of the two counter-rotating eddies, the valve eddy and the piston eddy, the latter forming because of the separation of the wall boundary layer.

The grid velocity and streamline plots indicate that the velocities are slightly smaller in this case than in the small-seat-angle case. The eddies are therefore weaker and their energy is dissipated faster. The results show qualitative similarity to the experimental results of Morse *et al.*[5]

4.3. A chamber fitted with an open centred valve

A more practical configuration, which is also more difficult to analyse than the previous cases because of its geometrical complexity, is a chamber fitted with an intake valve. When this valve is closed it is flush with the chamber head. During the intake stroke it is opened by moving the valve into the chamber very quickly to allow the fresh charge in without significant pressure loss. In the numerical simulations we assume that the valve is fully opened during the entire intake process. The distance between the valve seat and the chamber top is $l/d = 0{\cdot}5$ and the channel width measured along the chamber top is $d/D = 0{\cdot}15$.

Because the valve penetrates into the chamber, it forces the inlet jet to enter the chamber at the same angle as that of the inlet channel. In the case we analysed, the inlet channels are directed at an angle of 45° with respect to the chamber head, similar to the configuration which was used in

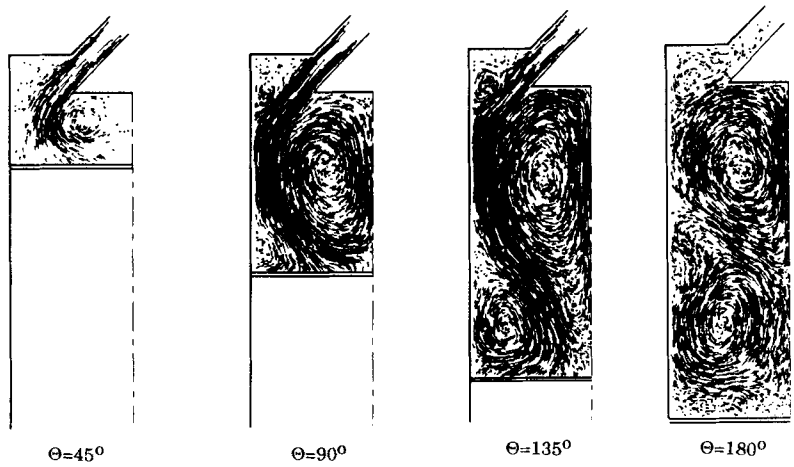

Figure 10. The symmetric flow field, depicted in terms of the vortex elements and their velocity vectors, for the intake flow in a planar piston–chamber device fitted with a centred intake valve at a seat angle of 45° with the chamber head, shown at equivalent crank angles $\theta = 45°$, 90°, 135° and 180°

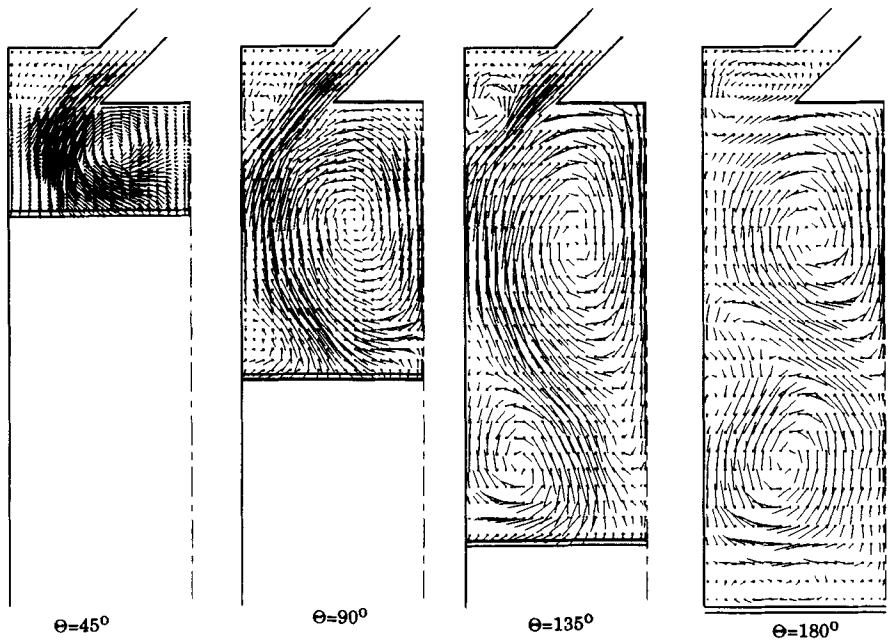

Figure 11. The symmetric flow field, exhibited in terms of the instantaneous velocity vectors on a uniform expanding grid, for the intake flow in a planar piston–chamber device fitted with a centred intake valve at a seat angle of 45° with the chamber head, presented at equivalent crank angles $\theta = 45°$, 90°, 135° and 180°

the experimental investigation of Ekchian and Hoult.[2] As indicated by the results in Figures 10–12, the flow dynamics is similar to that observed in the case of an intake port. The most important difference is the slight increase in the size of the corner eddy owing to the extra area it is allowed between the valve and the chamber head.

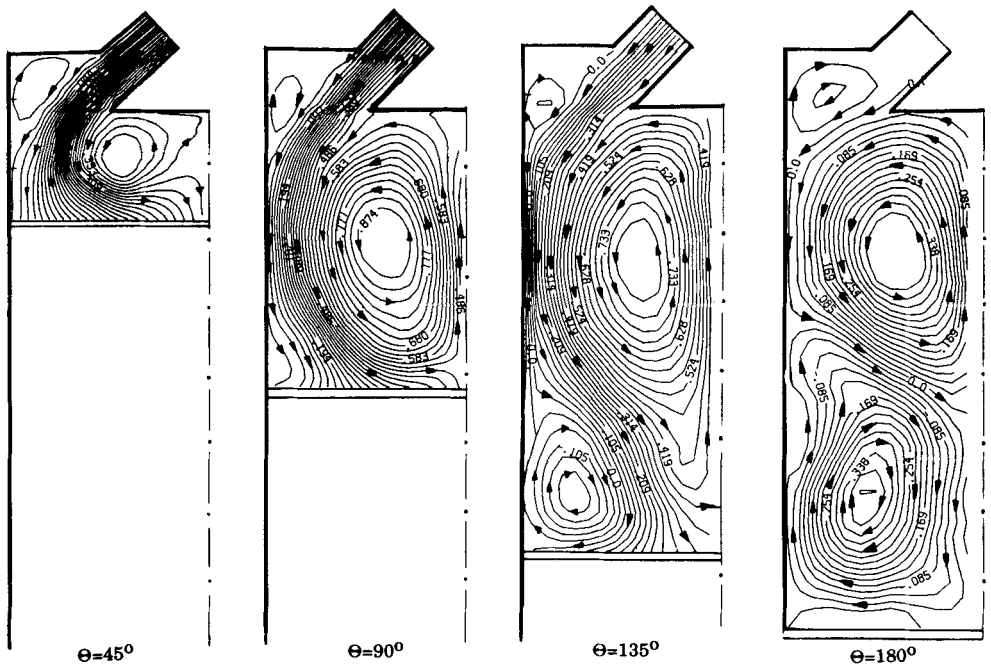

Figure 12. The symmetric flow field, illustrated by the instantaneous streamlines, for the intake flow in a planar piston–chamber device fitted with a centred intake valve at a seat angle of 45° with the chamber head, shown at equivalent crank angles $\theta = 45°$, 90°, 135° and 180°

Since the velocity at the inlet section of the intake channel is determined by the motion of the piston, the flow in this channel resembles that which was observed in the case of an intake port. As shown by the plots of the vortex elements and their velocity vectors in Figure 10, two boundary layers grow along the two side walls of the inlet channel, reaching their maximum thicknesses at $\theta = 90°$. The flow in the inlet channel carries all the vorticity produced within the two boundary layers into the chamber at a rate dependent on the piston speed. The inlet jet velocity is not affected by the sudden expansion between the inlet passage and the chamber because of the penetration of the valve seat and the formation of the valve eddy. As seen from the results, the separated boundary layers result in the formation of the corner eddy and the valve eddy.

In the case of an inlet port the corner eddy decays after $\theta = 90°$. In the case of an inlet valve, however, the corner eddy grows faster after half crank and fills more of the space between the chamber head and the intake valve. The corner eddy and the valve eddy rotate in opposite directions and the growth of the former affects the latter as seen in Figure 10. The inlet jet reaches higher velocities in this case since, owing to the presence of the corner eddy, the effective area of the intake is slightly reduced. Weak shear persists between the corner eddy and the valve eddy until the end of the stroke.

The intrusion of the valve seat into the chamber during intake promotes the early growth of the valve eddy by guiding the inlet jet towards the chamber walls instead of letting it move normal to the piston face as in the case of a port. As the piston passes the 90° crank angle the growth of the valve eddy is encumbered and the boundary layer which has been developing along the chamber walls separates to form a new eddy, the piston eddy. The separation of the boundry layer causes

the deflection of the inlet jet towards the centreline. The piston eddy and the valve eddy rotate in opposite directions, increasing the resistance to the penetration of the valve eddy into the expanding chamber. The establishment of a two-eddy system is very similar to what was previously observed in the intake port cases, which is shown in the streamline plots in Figure 12.

The presence of the valve and corner eddies at $\theta = 90°$ was revealed in the experiment of Ekchian and Hoult.[2]

4.4. A chamber fitted with a side port

So far, we have examined the flow structure produced by intake ports or valves which are symmetrically located with respect to the chamber centreline. In all cases the results show that the flow is formed of essentially four large eddies, two valve eddies and two piston eddies. Each two neighbouring eddies rotate in opposite directions. The so-called 'tumbling motion', defined as the coherent rotating fluid motion around an axis perpendicular to the cylinder axis, has recently received growing attention as a means of improving the mixing and enhancing the turbulence level in internal combustion engines.[36] This interest has been motivated in part by the increased utilization of two intake valves in three-valve or four-valve engines to improve the volumetric efficiency of the eigine. The source of the tumbling motion is believed to be the recirculating flow produced during the intake stroke when the inlet jets separate at the chamber head. In the following we will analyse results of an idealized model of this motion.

When the centreline of the intake port does not coincide with the chamber axis, results show that the flow field is completely different. Figures 13–15 depict results of a simulation of the flow during intake into a chamber equipped with a port whose centreline lies halfway between the chamber wall and the chamber axis. The angles of the inlet channels with respect to the chamber head are 30°, the widths of the inlet channels and the chamber are $d/D = 0{\cdot}1$ and the piston motion is as before. At the early stages and until $\theta = 45°$ the flow field is formed of two co-rotating eddies near the chamber head: the primary eddy on the right-hand side and the secondary eddy on the left-hand side. The primary eddy, so called since it will dominate the flow for the rest of the stroke, is formed owing to the separation of the inlet jet as it issues from the channel on the right side of the intake port. This jet moves into the chamber in a direction almost parallel to the

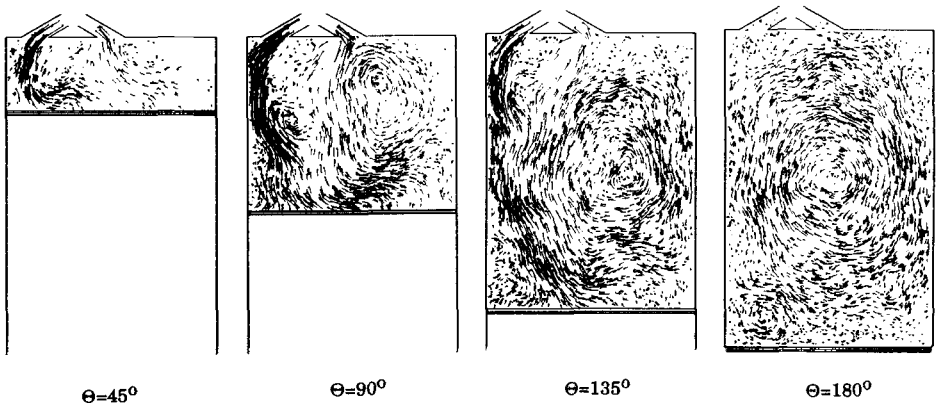

Figure 13. The flow field, depicted in terms of the vortex elements and their instantaneous velocity vectors, for the intake flow in a planar piston–chamber device fitted with an off-centred intake port at an equivalent seat angle of 30° with the chamber head, shown at equivalent crank angles $\theta = 45°$, 90°, 135° and 180°

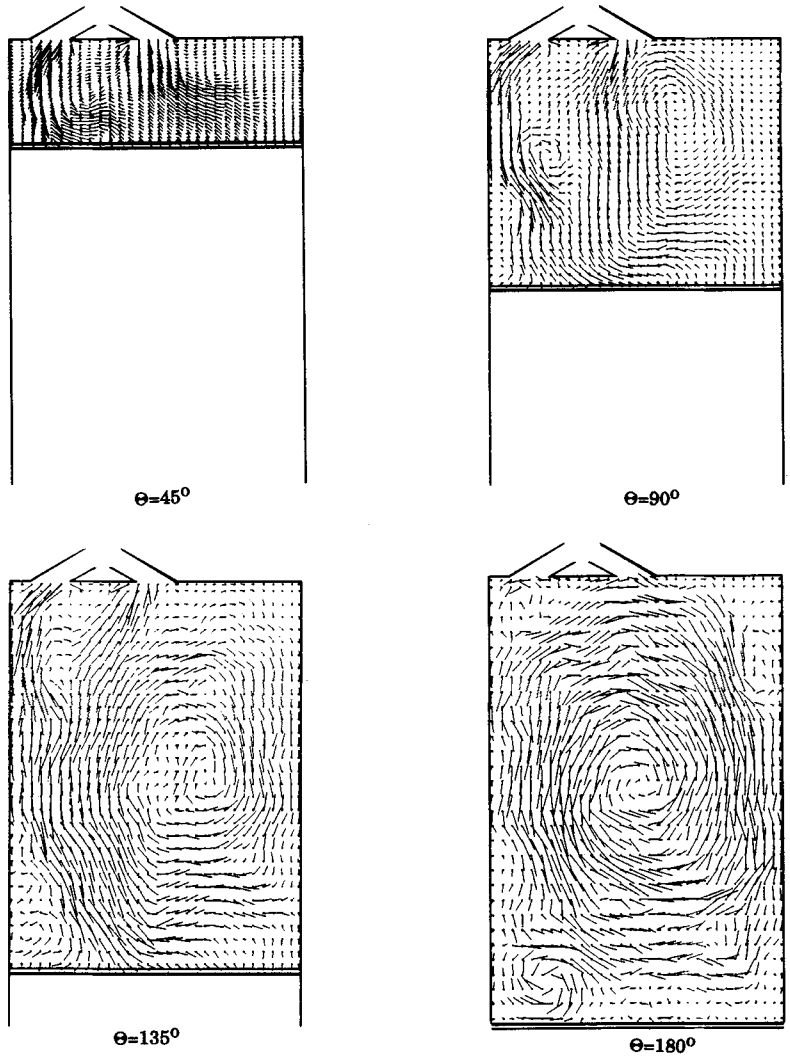

Figure 14. The flow field, exhibited in terms of the instantaneous velocity vectors on a uniform expanding grid, for the intake flow in a planar piston–chamber device fitted with an off-centred intake port at an equivalent seat angle of 30° with the chamber head, presented at equivalent crank angles $\theta = 45°$, 90°, 135° and 180°

direction of motion of the piston, similar to the inlet jet motion in the early stages in Section 4.2. The secondary eddy is formed, as seen from the plots of the vortex elements, owing to the deflection of the inlet jet on the left side of the intake port as it collides with the chamber wall.

It is interesting to point out that while the boundary conditions, in terms of the flow velocity, at the inlet sections of both channels are the same, the flow within both channels are not the same. This is because the conditions at the end of both channels, which are determined by the flow within the chamber, are not similar. The presence of a wall on the left side of the port acts as an obstacle which deflects the incoming flow. The vortex element distribution in Figure 13 shows that thicker boundary layers form on the walls of the channel on the left side than on the walls of

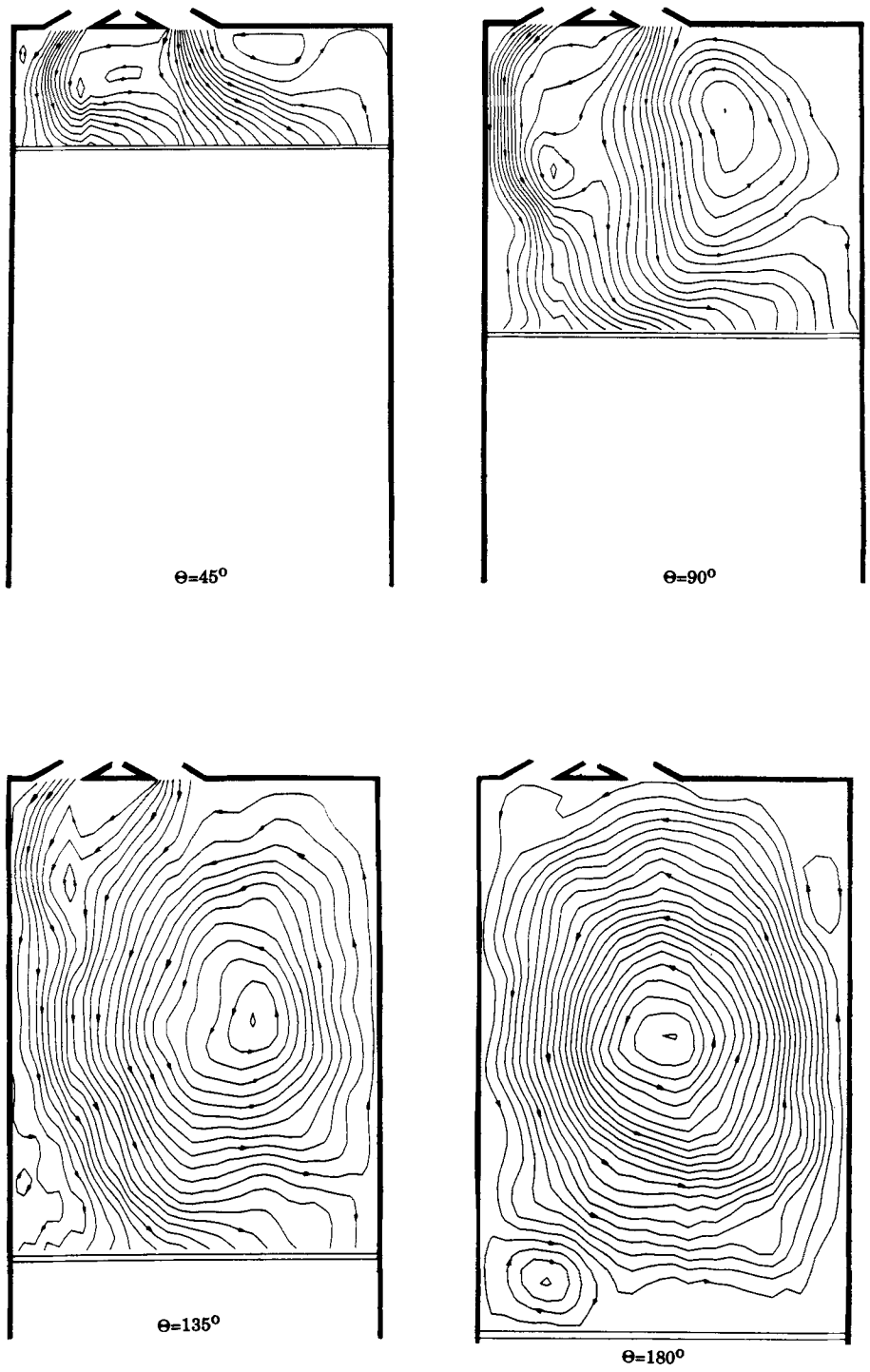

Figure 15. The flow field, illustrated by the instantaneous streamlines, for the intake flow in a planar piston–chamber device fitted with an off-centred intake port at an equivalent seat angle of 30° with the chamber head, shown at equivalent crank angles $\theta = 45°$, 90°, 135° and 180°

the channel on the right side. This is consistent with the fact that the exit of the channel on the left is more constrained by the presence of a wall than the exit of the channel on the right which is located almost halfway within the chamber. While the amount of vorticity generated in both channels is the same, its apparent concentration is higher in the jet coming through the left channel of the port. This is because the boundary layers are thicker in the left channel than in the right channel.

As the piston moves away from the chamber head, the primary eddy grows to fill the right side of the chamber while the secondary eddy moves along the chamber wall. As in previous cases, the motion of the jet along the wall leads to the formation of a boundary layer. Between $\theta = 90°$ and 135° the growth of the primary eddy fills the entire chamber, entraining the fluid coming through both channels. In the meantime, the separation of the boundary layer from the chamber wall as the piston is decelerating results in the formation of a small piston eddy. However, this eddy is too small and too weak to play a significant role in the dynamics of the flow. Between $\theta = 135°$ and the end of the stroke the inlet jets on both sides of the intake part are directly entrained into the primary eddy. At the end of the stroke a single eddy exists and the fluid within the chamber is 'tumbling' around a single centre of rotation. The sense of rotation of this eddy is determined by the location of the intake port with respect to the chamber centreline.

The difference between the flow fields produced by a centred intake port and an off-centre intake port is further illustrated by inspecting the grid velocity plots in Figure 14. The two eddies, which form on both sides of the intake port and circulate in the same direction, are shown at $\theta = 90°$. The merging of these two co-rotating eddies is accomplished within the range $90° > \theta > 135°$. It is interesting to see that at $\theta = 135°$ the two inlet jets merge beyond the port seat to form a single jet that feeds into the large eddy which fills the chamber. The piston eddy which appears around $\theta = 90°$ remains weak and small until the end of the stroke. Similar observations can be made from the plots of the streamlines in Figure 15.

5. DISCUSSION AND CONCLUSIONS

In this paper the flow inside a piston–chamber device fitted with different intakes is analysed using results of numerical solutions of the governing equations of the unsteady, incompressible, two-dimensional viscous flow. We use the vortex method to update the vorticity field and compute the rotational component of the velocity, and the finite element method to impose the boundary condition on the normal velocity and compute the potential component of the velocity. Using this idealized planar flow model we are able to obtain flow structures which strongly resemble the flow observed experimentally in axisymmetric configurations. While this resemblance is qualitative at this stage, it is hoped that the results will shed some light on the essential mechanisms of confined vortex flows and will encourage the development of more elaborate numerical schemes to compute axisymmetric and three-dimensional flows.

To our knowledge, this paper shows the first application of the vortex method in which the no-slip boundary condition is satisfied on boundary walls which are inclined with respect to the co-ordinate system. The consideration of large area ratios across the sudden expansion between the inlet channel and the main chamber, corners at which the flow separation angle is on one side smaller and on the other side larger than $3\pi/2$, and moving corners between the chamber walls and the piston face are also new features in the application considered in this paper. The algorithms developed to accommodate these complexities extend the application of the vortex method to a wide range of practically important flows. Although not presented here, these extensions include flows inside fully enclosed chambers whose volumes change slowly with time.[37,38]

Using the finite element method to solve the potential flow problem, which arises in the satisfaction of the conditions imposed on the velocity normal to the boundaries of the computational domain, provides great convenience in obtaining solutions for complex geometries. The method offers flexibility in allowing one to solve the potential flow problem in a domain defined by a large number of walls which intersect at arbitrary angles, and to change the geometry of the boundaries without substantial modifications of the main code. Previous applications were limited to domains with known conformal transformations, or simple domains for which fast potential solvers exist. This flexibility was used in a parametric study to investigate the effect of the intake geometry on the flow inside the chamber.

The expanding computational domain, defined by the moving piston and the chamber, requires that the stiffness matrix be updated every time step. This extra computational effort can be avoided in the application of the method to a domain with a fixed geometry.[37] The cost of updating the stiffness matrix is, however, much smaller than that of computing vortex interactions. The expanding domain also means that one must generate vortex sheets with different lengths on the walls at different time steps, assuming that the number of points where the no-slip condition is satisfied is constant. The vortex sheet algorithm was accordingly modified. The vortex blobs in the domain also have different core radii since they are generated from vortex sheets with different lengths. In the case of an incompressible flow the core radii of the blobs stay constant.

Results show that in all cases the confined vortical flow inside the chamber is dominated by a small number of large vortices which are generated owing to the separation of the incoming jet around the sudden expansion between the inlet channel and the chamber, and the separation of the boundary layer which forms along the chamber walls as a result of the jet flow and the valve vortices. The size, location and direction of rotation of these structures depend strongly on the intake configuration. The separation of the incoming jet leads to the formation of a strong eddy that grows for the most part of the stroke. The separation of the boundary layer leads to the formation of a second eddy during the latter part of the stroke.

In cases when the intake is symmetrical around the centreline of the chamber, the flow field at the end of the stroke consisted of four eddies, two on each side of the centreline. The two eddies rotate in opposite directions. The 'tumbling' motion around an axis normal to that of the chamber was observed in the case of the off-centred port. In this case the field is dominated by a single eddy that fills the entire chamber volume and captures the whole charge. The detail of this structure is expected to depend on the dimensionality of the chamber, and the results of the current two-dimensional planar calculations must be taken as an indication that, provided there is more than one intake port, one should expect rotation in the plane of the chamber axis. The axis of the rotation is normal to the plane of the flow.

The computational model is currently being extended to a two-dimensional axisymmetric flow inside a piston–cylinder device.[37] Using vortex rings in place of the rectilinear vortex blobs and extending the potential solver to accommodate the axisymmetric domain will allow us to study the effect of the flow dimensionality on the vortex structures. We are also working on extending the simulation algorithms, on the basis of the three-dimensional vortex method,[39] to compute three-dimensional flow inside a piston–cylinder device.

REFERENCES

1. E. Krause, 'Computation of confined vortical flow', *Ann. Rev. Numer. Fluid Mech. Heat Transfer*, **II**, 256–284 (1989).
2. A. Ekchian and D. P. Hoult, 'Flow visualization study of the intake proces of an internal combustion engine', *SAE Paper No. 790095, SAE Congress and Exposition*, Detroit, MI, 1979, *Trans. SAE*, 1196–1216 (1981).
3. H. Henke and D. Hanel, 'Numerical simulation of gas motion in piston engines', *Proc. 9th Int. Conf. on Numerical Methods in Fluid Dynamics, Lecture Notes in Physics, Vol. 218*, Springer, Berlin, 1985, pp. 267–271.

4. F. Durst, T. Maxworthy and J. C. F. Pereira, 'Piston-driven, unsteady separation of a sudden expansion in a tube: flow visualization and LDA measurements', *Phys. Fluids*, **A1**, 1249–1260 (1989).
5. A. P. Morse, J. H. Whitelaw and M. Yianneskis, 'Turbulent flow measurements by laser–Doppler anemometry in motored piston–cylinder assemblies', *ASME J. Fluids Eng.*, **101**, 208 (1979).
6. C. Arcoumanis, A. F. Bicen, N. S. Vlachos and J. H. Whitelaw, 'Effect of flow and geometry boundary conditions on fluid motion in a motored IC engine', *Proc. Inst. Mech. Eng.*, **169**, 1–10 (1982).
7. L. F. Martins and A. F. Ghoniem, 'Vortex simulation of the induction and compression processes in an engine model', *SAE Paper No. 872102, Internal Fuels and Lubricants Meeting and Exposition*, Toronto, Ontario, 2–5 November 1987.
8. A. J. Chorin, T. Hughes, M. McCracken and J. Marsden, 'Product formulas and numerical algorithms', *Commun. Pure Appl. Math.*, **31**, 205–256 (1978).
9. J. T. Beale and A. Majda, 'Rates of convergence for viscous splitting of the Navier–Stokes equations', *Math. Comput.*, **37**, 243–259 (1981).
10. A. J. Chorin, 'Numerical study of slightly viscous flow', *J. Fluid. Mech.*, **57**, 785–796 (1983).
11. A. F. Ghoniem and F. S. Sherman, 'Grid-free simulation of diffusion using random walk methods', *J. Comput. Phys.*, **61**, 1–37 (1985).
12. O. C. Zienkiewicz and K. Morgan, *Finite Elements and Approximation*, Wiley, New York, 1983, p. 126.
13. A. J. Chorin, 'Vortex sheet approximation of boundary layers', *J. Comput. Phys.*, **27**, 428–442 (1978).
14. A. J. Chorin, 'Vortex models and boundary layer instability', *SIAM J. Sci. Stat. Comput.*, **1**, 1–21 (1980).
15. A. F. Ghoniem and Y. Gagnon, 'Vortex simulation of laminar recirculating flow', *J. Comput. Phys.*, **68**, 346–377 (1987).
16. O. M. Hald, 'Convergence of vortex methods for Euler's equations: II', *SIAM J. Numer. Anal.*, **16**, 726–755 (1979).
17. J. T. Beale and A. Majda, 'Vortex methods II: higher order accuracy in two and three dimensions', *Math. Comput.*, **39**, 28–52 (1982).
18. C. Marchioro and M. Pulvirenti, *Vortex Methods in Two Dimensions, Lectures Notes in Physics, Vol. 203*, Springer, Berlin, 1984, 137 p.
19. D. C. Long, 'Convergence of the random vortex method in two dimensions', *Preprint*, 1988.
20. O. Hald, 'Convergence of a random method with creation of vorticity', *PAM-270*, Center for Pure and Applied Mathematics, University of California, Berkeley, CA, 1985.
21. S. Roberts, 'Accuracy of the random vortex method for a problem with non-smooth initial conditions', *J. Comput. Phys.*, **58**, 24–43 (1985).
22. E. G. Puckett, 'A study of the vortex sheet method and its rate of convergence', *SIAM J. Sci. Stat. Comput.*, **10**, 298–327 (1989).
23. J. A. Sethian and A. F. Ghoniem, 'Validation of the vortex method', *J. Computer. Phys.*, **74**, 283–317 (1988).
24. A. F. Ghoniem and K. K. Ng, 'Numerical study of the dynamics of a forced shear layer', *Phys. Fluids*, **30**, 706–721 (1987).
25. H. Najm, and A. F. Ghoniem, 'Numerical simulation of the convective instability in a dump', *AIAA Paper No. 87-1874, AIAA/SAE/ASME/ASEE 23rd Joint Propulsion Conf.*, La Jolla, CA, 29 June–1 July 1979.
26. W. T. Ashurst, 'Vortex simulation of a model turbulent combustor', *Proc. 7th Colloq. on Gas Dynamics of Explosions and Reactive Systems, Prog. Astronaut. Aeronaut.*, **76**, 259–273 (1981).
27. C. Peskin and M. McCracken, 'Vortex methods for blood flow through heart valves', *J. Comput. Phys.* **35**, 183–205 (1979).
28. A. Y. Cheer, 'Unsteady separated wake behind an impulsively started cylinder in slightly viscous flow', *J. Fluid Mech.*, **201**, 485–506 (1989).
29. W. T. Ashurst, 'Vortex dynamic calculation of fluid motion in four stroke piston 'cylinder'—planar and axisymmetric geometry', *Sandia Laboratory Report SAND79-8229*, 1979.
30. J. A. Sethian, 'Turbulent combustion in open and closed vessels', *J. Comput. Phys.*, **55**, 425 (1984).
31. G. A. Sod, 'Automotive engine modeling with a hybrid random choice method', *SAE Paper 790242*, Detroit, MI, 1979.
32. G. A. Sod, 'Automotive engine modeling with a hybrid random choice method II', *SAE Paper 800288*, Detroit, MI, 1979.
33. Y. Choi, J. A. C. Humphrey and F. S. Sherman, 'Random vortex simulations of transient wall driven flow in a rectangular cavity', *J. Comput Phys.*, **75**, 359–383 (1988).
34. A. D. Gosman, 'Flow processes in cylinders', in J. Horlock and D. Winterborne (eds), *Thermodynamics and Gas Dynamics of Internal Combustion Engines*, Vol. II, Clarendon Press, Oxford, 1983, pp. 616–772.
35. S. H. El-Tahry, 'A comparison of three turbulence models in engine-like geometries', *Proc. Int. Symp. on Diagnostics and Modeling of Combustion in Reciprocating Engines, COMODIA 85*, JSME, Tokyo, 1985, pp. 203–213.
36. J. C. Kent, A. Mikulec, L. Rimai, A. A. Adamczyk, S. R. Mueller, R. A. Stein and C. C. Warren, 'Observations on the effects of intake-generated swirl and tumble on combustion duration', *SAE Fuel and Lubricants Meeting*, Baltimore, MD, 25–28 September 1989.
37. L.-F. Martins, 'Vortex computations of axisymmetric high Reynolds number flows in complex domains', *Ph.D. Thesis*, Massachusetts Institute of Technology, 1990.
38. T. Bress 'The effect of squish–piston geometry on flame propagation', *M.Sc. Thesis*, Massachusetts Institute of Technology, 1989.
39. O. M. Knio and A. F. Ghoniem, 'Numerical study of a three dimensional vortex scheme', *J. Comput. Phys.*, **86**, 75–106 (1990).